



# Evidence from giant-clam $\delta^{18}\text{O}$ of intense El Niño–Southern Oscillation-related variability but reduced frequency 3700 years ago

Yue Hu<sup>1,2</sup>, Xiaoming Sun<sup>1,2,3,4</sup>, Hai Cheng<sup>5,6</sup>, and Hong Yan<sup>7,8,9</sup>

<sup>1</sup>School of Marine Sciences, Sun Yat-sen University, Guangzhou 510006, China

<sup>2</sup>Guangdong Provincial Key Laboratory of Marine Resources and Coastal Engineering, Guangzhou 510275, China

<sup>3</sup>School of Earth Sciences and Engineering, Sun Yat-sen University, Guangzhou 510275, China

<sup>4</sup>Southern Marine Science and Engineering Guangdong Laboratory (Zhuhai), Zhuhai 519000, China

<sup>5</sup>Institute of Global Environmental Change, Xi'an Jiaotong University, Xi'an 710054, China

<sup>6</sup>Department of Earth Sciences, University of Minnesota, Minneapolis, Minnesota 55455, USA

<sup>7</sup>State Key Laboratory of Loess and Quaternary Geology, Institute of Earth Environment, Chinese Academy of Sciences, Xi'an 710061, China

<sup>8</sup>CAS Center for Excellence in Quaternary Science and Global Change, Xi'an 710061, China

<sup>9</sup>OCCES, Qingdao National Laboratory for Marine Science and Technology, Qingdao 266061, China

**Correspondence:** Xiaoming Sun (eessxm@mail.sysu.edu.cn) and Hong Yan (yanhong@ieecas.cn)

Received: 10 May 2019 – Discussion started: 3 June 2019

Revised: 6 February 2020 – Accepted: 20 February 2020 – Published: 1 April 2020

**Abstract.** Giant clams (*Tridacna*) are the largest marine bivalves, and their carbonate shells can be used for high-resolution paleoclimate reconstructions. In this contribution,  $\delta^{18}\text{O}_{\text{shell}}$  was used to estimate climatic variation in the Xisha Islands of the South China Sea. We first evaluate sea surface temperature (SST) and sea surface salinity (SSS) influence on the modern resampled monthly (*r*-monthly) resolution of *Tridacna gigas*  $\delta^{18}\text{O}_{\text{shell}}$ . The results obtained reveal that  $\delta^{18}\text{O}_{\text{shell}}$  seasonal variation is mainly controlled by SST and appears to be insensitive to local SSS change. Thus, the  $\delta^{18}\text{O}$  of *Tridacna* shells can be roughly used as a proxy of local SST: a 1‰  $\delta^{18}\text{O}_{\text{shell}}$  change is roughly equal to 4.41 °C of SST. The *r*-monthly  $\delta^{18}\text{O}$  of a 40-year-old *Tridacna squamosa* (3673 ± 28 BP) from the North Reef of the Xisha Islands was analyzed and compared with the modern specimen. The difference between the average  $\delta^{18}\text{O}$  of the fossil *Tridacna* shell ( $\delta^{18}\text{O} = -1.34\text{\textperthousand}$ ) and the modern *Tridacna* specimen ( $\delta^{18}\text{O} = -1.15\text{\textperthousand}$ ) probably implies a warm climate, roughly 0.84 °C, 3700 years ago. The seasonal variation 3700 years ago was slightly lower than that suggested by modern instrumental data, and the transition between warm and cold seasons was rapid. Higher amplitudes

of reconstructed *r*-monthly and *r*-annual SST anomalies imply an enhanced climate variability during this warm period. Investigation of the El Niño–Southern Oscillation (ENSO) variation (based on the reconstructed SST series) indicates reduced ENSO frequency but increased ENSO-related variability and extreme El Niño winter events 3700 years ago.

## 1 Introduction

The carbonate skeletons of marine organisms, such as corals, foraminifers, and mollusks, have been widely used to reconstruct environmental variation (Aharon, 1983; Batenburg et al., 2011; Ourbak et al., 2006; Schöne et al., 2005; Wanamaker et al., 2011; Yamanashi et al., 2016; Yu et al., 2005a, b). Due to their high sensitivity to the surrounding environment and the fact that they preserve high-resolution biochemical variations in their skeleton, these marine biogenic carbonates can shed light on past climate dynamics. Bivalves, which are considered to be high-resolution records, can give us more precise details on environmental variation. Giant clams (*Tridacna*), as they are the largest bivalves and usually

live in tropical coral reefs, have received increasing scientific attention in recent decades (Pätzold et al., 1991; Watanabe et al., 1999, 2004; Elliot et al., 2009; Ayling et al., 2015; Agbaje et al., 2017). This is because their shells have many favorable properties for recording local environmental changes: they have dense and well-preserved aragonite shells, fast growth rates (up to  $1\text{ cm yr}^{-1}$ ) with clear annual growth lines, and a longevity of several decades to about 100 years. These characteristics allow *Tridacna* to provide ideal material for high-resolution reconstruction of interannual, seasonal, or even subseasonal climatic variations.

Previous studies indicate that *Tridacna* species grow their shells in oxygen isotopic ( $\delta^{18}\text{O}$ ) equilibrium with the surrounding seawater (Aharon, 1991; Aharon and Chappell, 1986; Pätzold et al., 1991; Romanek and Grossman, 1989; Watanabe et al., 1999). The reliability of reconstructing temperature and seawater  $\delta^{18}\text{O}$  variability is not reduced and does not show obvious increasing or decreasing trends due to *Tridacna*'s ontogenetic growth (Welsh et al., 2011). These studies imply that  $\delta^{18}\text{O}_{\text{shell}}$  can be used to reconstruct Late Quaternary sea-level and climatic changes. Indeed, the  $\delta^{18}\text{O}$  of marine biogenic carbonates is influenced not only by sea surface temperature (SST) but also by surrounding seawater  $\delta^{18}\text{O}$ . Meanwhile, seawater  $\delta^{18}\text{O}$  has a close correlation with sea surface salinity (SSS), which is affected by tropical evaporation and the precipitation balance. Nonetheless, the influence of SST and SSS on  $\delta^{18}\text{O}_{\text{shell}}$  is unclear due to the distinct variation of temperature and salinity in different areas. For example, the  $\delta^{18}\text{O}_{\text{shell}}$  of *Tridacna* from southwestern Japan can be directly used as a proxy of SST (Yamanashi et al., 2016), while the  $\delta^{18}\text{O}_{\text{shell}}$  of Indonesian *Tridacna* has been interpreted to be a contribution of 71.4 % from SST and 28.6 % from SSS (Arias-Ruiz et al., 2017). Thus, local calibration from modern *Tridacna* is important in determining the relationship of  $\delta^{18}\text{O}_{\text{shell}}$ , SST, and SSS.

Climatic variation in the Meghalayan (which began 4200 BP in the Late Holocene) has significant impacts on human society and ecosystem development. However, early Meghalayan climatic conditions in SE Asia around the South China Sea still remain poorly understood. Shi (1994) reviewed data from various sources (such as ice cores, inland lakes, paleosols in loess and eolian sands, sea-level fluctuations, palynological and botanical studies) in China and found that the early Meghalayan is a part of the Holocene megathermal period (8 to 3 kyr BP). Sediments in the South China Sea also imply that the temperature might have been relatively higher in the early Meghalayan than in the present (Ouyang et al., 2016). However, these studies are low-resolution, and high-resolution records under interannual climate variation are rare. With global warming and numerous climatic disasters happening in recent decades, climatic conditions in the early Meghalayan could serve as an analogue to modern problems and have received increasing scientific attention (Schirrmacher et al., 2019; Scuderi et al., 2019; Toth and Aronson, 2019; Zhang et al., 2018). Recent studies of bi-

valve mollusk specimen (*Arctica islandica*) oxygen isotopes show high-resolution data with seasonal signals (Schöne et al., 2005; Wanamaker et al., 2011). High-resolution isotopic geochemical data from *Tridacna* may also provide detailed insight into climatic variations in the early Meghalayan.

Furthermore, El Niño–Southern Oscillation (ENSO) is widely accepted as the main source of interannual climatic variability in the Pacific Ocean. Previous studies suggest that the impacts of ENSO activity are not limited to tropical areas but might also apply to global atmospheric circulation through the heating-up of the tropical atmosphere (Cane, 2005). Thus, reconstructing ENSO is very important for understanding its dynamics and predicting future change. Many early studies on ENSO behaviors were constructed with low-resolution proxy data using deposition events (Rodbell et al., 1999; Koutavas and Joanides, 2012) or ice cores (Thompson et al., 1995) in order to reveal ENSO variance over thousands of years. However, the periodicity of ENSO is short, making it difficult to use these low-resolution data to precisely determine the strength and variability of ENSO activity. Recent studies focus on seasonal or monthly data to examine precise variation of ENSO activity (Arias-Ruiz et al., 2017; Ayling et al., 2015; McGregor et al., 2013; Welsh et al., 2011; Yan et al., 2017), but those fragmental data cannot fully explain the Holocene ENSO dynamics. Therefore, fragments from different times according to different high-resolution samples are needed and can provide an integrated framework for examining ENSO theory and models of the Holocene. In addition, studies on the Middle to Late Holocene ENSO evolution yield controversial findings: coral records show a reduced ENSO variability around the early Meghalayan (Tudhope et al., 2001; McGregor et al., 2013; Cobb et al., 2014; Woodroffe et al., 2003). Other carbonate species like fossil mollusk shells suggest that ENSO variance was severely damped  $\sim 4000$  years ago (Carré et al., 2014). Yet other studies indicate strengthening ENSO activity at 4 to 3 ka (Duprey et al., 2014; Yang et al., 2019). Thus, this further points to the importance of high-resolution isotopic geochemical data such as from *Tridacna* in unraveling the dynamics of ENSO.

This study aims to evaluate seasonality, climate variation, and ENSO activity in the Xisha Islands of the northern South China Sea, based on two high-resolution  $\delta^{18}\text{O}_{\text{shell}}$  profiles of modern and fossil *Tridacna*. The study area is situated in the northwest margin of the west Pacific warm pool (WPWP), and the local climate is widely accepted to be directly responsive to ENSO activity (Mitsuguchi et al., 2008; Yan et al., 2010). A modern *Tridacna gigas* shell was first used to estimate the extent of environmental control (SST and SSS) on  $\delta^{18}\text{O}_{\text{shell}}$ , and a new SST– $\delta^{18}\text{O}_{\text{shell}}$  linear regression was proposed. Subsequently, a fossil *Tridacna squamosa* (which lived to 40 years) was used to reconstruct seasonality and climatic variation, and the obtained results are compared with the modern species and meteorological observations. Finally,

ENSO activity and extreme El Niño winter events were discussed, using the re-established SST anomalies.

## 2 Materials and methods

### 2.1 Regional setting

The South China Sea is located in the northwest of WPWP (Fig. 1a), and its interannual climate is closely related to ENSO activities (Mitsuguchi et al., 2008; Yan et al., 2010). The Xisha Islands in the northern South China Sea are substantially influenced by two contrasting Asian monsoons from opposite directions: the Asian summer monsoon from the southwest and the Asian winter monsoon from the northeast. These two monsoons provide distinct seasonal SST for the *Tridacna* populating the coral reefs of the Xisha Islands. Our sample (*Tridacna squamosa* A5) was collected in the North Reef ( $17^{\circ}05'\text{N}$ ,  $111^{\circ}30'\text{E}$ ), whilst the modern *Tridacna gigas* sample YX1 (studied previously by Yan, 2013) was acquired from Yongxing Island ( $16^{\circ}50'\text{N}$ ,  $112^{\circ}50'\text{E}$ ), which is about 90 km away from the North Reef (Fig. 1b).

Meteorological observations (atmosphere temperature, AT; SST; SSS; rainfall) were obtained from the Institute of Meteorology of China, which has taken records for the Xisha Islands since 1958. In order to compare geochemical analyses with monthly environmental data, isotopic records and meteorological observations were resampled according to the method suggested by Schöne and Fiebig (2009). They used bivalve shells (*Arctica islandica*) to reconstruct the climate, examining that seven points per year would minimize the influence of different growth rates throughout the year; meanwhile, only the annual sample number for which more than or equal to seven existed could be used. As the yearly minimum number of  $\delta^{18}\text{O}_{\text{YX1}}$  is seven, 1 year includes 7 resampled months ( $r$  months). Figure 1d shows the  $r$ -monthly average time series of AT, SST, SSS, and rainfall, and their standard deviations (SDs). The mean SST is  $27.77^{\circ}\text{C}$ , and AT shows a highly positive correlation with SST ( $r = 0.98$ ), but it is about  $0.7^{\circ}\text{C}$  lower. The SST seasonality is  $5.33^{\circ}\text{C}$ , with the lowest value and highest value occurring in first and fourth  $r$  months, respectively. It is excluded that river runoff effects on SSS as the Xisha Islands are about 300 km away from the continent (Hainan Island). SSS varies from  $33.25\text{‰}$  to  $33.81\text{‰}$ , and the change is mainly dominated by rainfall: higher SSS in dry winters and lower SSS in wet summers (Fig. 1e).

The SST data in the North Reef are acquired from NOAA HadISST, a global monthly SST data with a spatial resolution of  $1 \times 1^{\circ}$  (data grid cell includes both the North Reef and Yongxing Island) from 1982 to 2017. Ninō 1 + 2 SST data are obtained from NOAA monthly data between 1982 and 2017 (<http://www.cpc.ncep.noaa.gov/data/indices/sstoi.indices>; last access: 31 December 2017).

### 2.2 Shell descriptions and sample preparation

The original fossil *Tridacna* was cut from the umbo to the ventral (red line in Fig. 1b), where the thickness of the inner layer is the greatest. From the slice we cut, the fossil *Tridacna* has three different zones (Fig. 1c): the inner layer, the outer layer, and the hinge. A recent study investigating the architecture of *Tridacna* shells shows a crossed lamellar microstructure with a strong fiber texture with optimized mechanical performance (Agbaje et al., 2017), and the mineralization of inner layer and outer layer is independent of each other (Gannon et al., 2017). The inner layer is chosen for the analyses because of its clear growth layer and well-preserved shell. Published data also reveal that inner layer  $\delta^{18}\text{O}$  values are unaffected by ontogeny (Welsh et al., 2011) and could better reflect actual  $\delta^{18}\text{O}$  than the outer layer or the hinge (Pätzold et al., 1991; Elliot et al., 2009).

The determination of radiocarbon age was performed at the Institute of Earth Environment of Chinese Academy of Sciences. The  $^{14}\text{C}$  accelerator mass spectrometry data revealed that the fossil *Tridacna gigas* age is  $3437 \pm 28$  yr BP. Due to the lack of an obvious “reservoir effect” in the dating results of modern *Tridacna* shells, the atmospheric  $^{14}\text{C}$  yield model is used for calibration (Liu et al., 2019). The calibrated date ( $2\sigma$ ) ranges from 3733 to 3613 cal BP, with the median date is 3691 cal BP by using the IntCal13 of Radiocarbon Calibration Program CALIB 7.10 (<http://calib.org>, last access: 31 December 2018). Both X-ray diffraction (XRD) and laser Raman spectrometers results show aragonite, and no other substances are found.

### 2.3 Stable isotopes

Each stable isotope sample was micromilled parallel to the growth layer with 1 mm long and  $100\text{ }\mu\text{m}$  deep under a micro-drill automated system (Micro-Drill New Wave Research, Olympus SZ 61) in the Isotope Laboratory of Xi'an Jiaotong University, China. Four intervals were used according to the growth rates:  $100\text{ }\mu\text{m}$  ( $n = 1$  to 268),  $150\text{ }\mu\text{m}$  ( $n = 269$  to 481),  $200\text{ }\mu\text{m}$  ( $n = 482$  to 657), and  $300\text{ }\mu\text{m}$  ( $n = 658$  to 765) in a transect from adult to ontogenetically younger shell, respectively (Fig. 2a).

The  $\delta^{18}\text{O}$  of the *Tridacna* was analyzed in the Isotope Laboratory of Xi'an Jiaotong University, using the Thermo Finnigan MAT-253 mass spectrometer fitted with the Kiel IV Carbonate Device. All results were reported in per mil (‰), relative to the Vienna Pee Dee Belemnite (VPDB) standard. The standard GBW04405, which has been compared with international standard NBS-19, was added to the analyses every 10 to 20 samples to check reproducibility. The average value of standard powder in  $\delta^{18}\text{O}$  is  $-8.49 \pm 0.14\text{ ‰}$ . Duplicate measurements of GBW04405 standards and samples showed long-term reproducibilities ( $1\sigma$ ) of less than  $0.14\text{ ‰}$  and  $0.05\text{ ‰}$ , respectively.

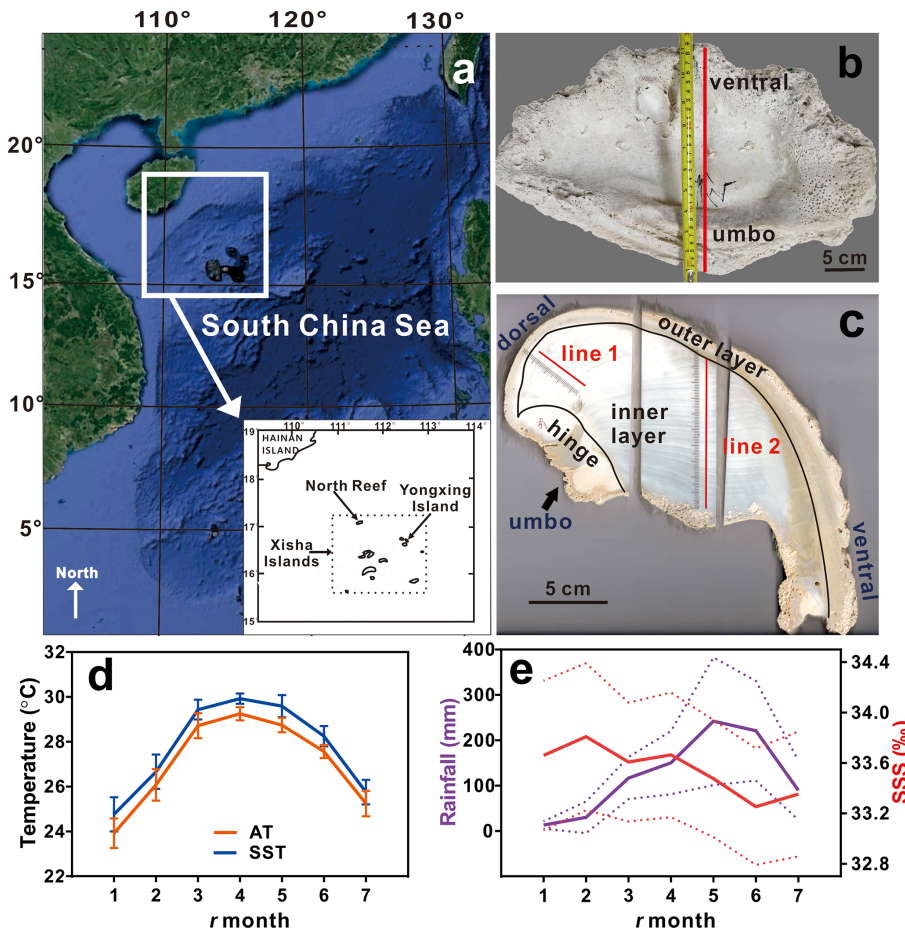


**Figure 1.** (a) Maps of the South China Sea (source: © Google Maps), with the location of the sample study area in the Xisha Islands. (b) Photo of original *Tridacna* A5. A slice was cut through the red line of *Tridacna* A5. (c) From the slice, different parts can be seen (hinge, inner layer, and outer layer); the red lines are the sampling lines for  $\delta^{18}\text{O}$  analysis. (d) Meteorological observations from the Xisha Islands from 1994 to 2005; *r*-monthly average air temperature (AT) and sea surface temperature (SST) with error bars revealing the highest and the lowest temperatures for that month; (e) *r*-monthly average rainfall and sea surface salinity (SSS) with a standard deviation ( $1\sigma$ ).

Published data of the modern *Tridacna gigas* shell YX1 were used to investigate the relationship between *Tridacna*  $\delta^{18}\text{O}$  and the local climate (Yan et al., 2013). YX1 was collected from Yongxing Island, 90 km ESE of the North Reef (Fig. 1b). The internal carbonate standard of modern *Tridacna* YX1  $\delta^{18}\text{O}$  (VPDB) was also GBW04405; the standards and samples had reproducibilities ( $1\sigma$ ) of better than 0.08 ‰ and 0.06 ‰, respectively.

#### 2.4 Data processing and analyses

PearsonT3 (Version 2.2, January 2017) was used to test the correlation coefficient. Successive sets of 100 years' length were calculated to estimate monthly insolation using the software AnalySeries 2.0.8 (Laskar et al., 2004), which contained the probable life span of *Tridacna* (A5) considering  $2\sigma$  confidence intervals of corrected age. The timescale of modern insolation ranges from 1918 to 2017, while the past ranges from 3722 to 3623 BP. Statistical analyses were per-

formed with the software Origin 2018 and PAST (Paleontological Statistics) 3.18. The isotopic records, meteorological observations, and insolation data were resampled for seven points per year using the software AnalySeries 2.0.8, as used for other studies in sclerochronology (Schöne and Fiebig, 2009; Wanamaker et al., 2011).

### 3 Results

#### 3.1 $\delta^{18}\text{O}_{\text{A}5}$ record

Seasonal cycles are distinct in the  $\delta^{18}\text{O}_{\text{A}5}$  profile (Fig. 2, Table S2), which indicate that this *Tridacna* lived for 40 years. The  $\delta^{18}\text{O}_{\text{A}5}$  range from  $-2.07\text{‰}$  to  $-0.14\text{‰}$  (mean  $-1.35\text{‰}$ ,  $n = 765$ ). After resampling into seven points per year,  $\delta^{18}\text{O}_{\text{A}5}$  varied from  $-1.98\text{‰}$  to  $-0.29\text{‰}$  (mean  $-1.34\text{‰}$ ,  $n = 281$ ).

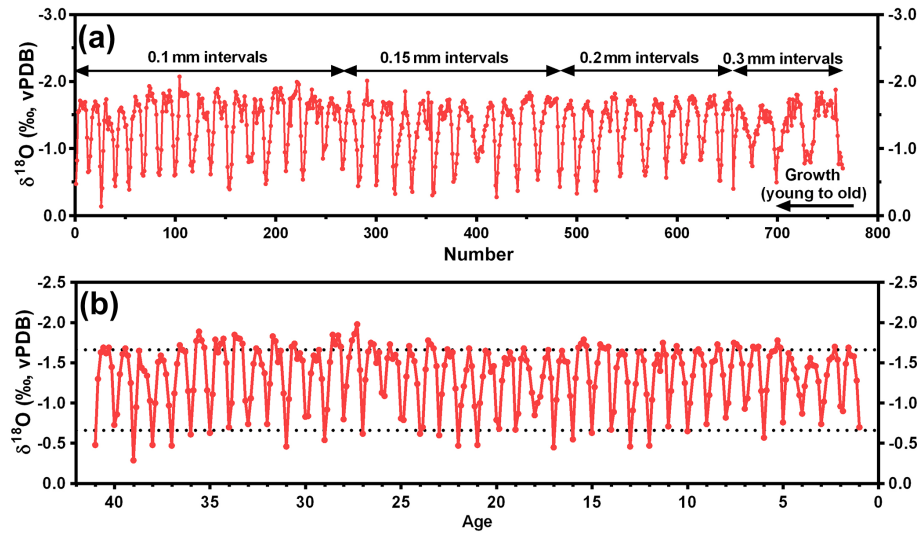


**Figure 2.** (a) The  $\delta^{18}\text{O}$  profiles of A5. (b) The  $\delta^{18}\text{O}_{\text{A5}}$  profiles chronology scale after resampling the data; the dotted lines indicate the average annual maximum and minimum.

### 3.2 Sclerochronology

From the shell section, dark–bright line couples (each couple represents 1 year) can be seen clearly (Fig. 3a). Following the  $\delta^{18}\text{O}_{\text{A5}}$  profiles, these short, dark lines (transparent) correspond to higher  $\delta^{18}\text{O}_{\text{A5}}$  values, which means that *Tridacna* grew in lower temperature (cold seasons such as December to February). In contrast, lower  $\delta^{18}\text{O}_{\text{A5}}$  values lie in the long bright lines (opaque), corresponding to the higher temperatures (warm seasons such as March to November). Annual growth rates can be calculated with the  $\delta^{18}\text{O}_{\text{A5}}$  seasonal cycles and interval distance (Fig. 3c). The results show that growth rates were higher when *Tridacna* A5 was young, reaching  $5 \text{ mm yr}^{-1}$ . The growth then slowed down and stabilized to  $1\text{--}2 \text{ mm yr}^{-1}$  after the *Tridacna* had matured (Fig. 3c). Furthermore, daily increments visible as pairs of dark and bright increments can be seen under the microscope (Fig. 3b). A fragment was chosen where  $\delta^{18}\text{O}$  values were nearly the highest in a particular year. This period fell during the cold season, when the daily growth increment was about  $4.5 \mu\text{m}$ . When the temperature rose as warm season began, *Tridacna* grew faster, with daily growth increment reaching up to  $8 \mu\text{m}$ . This situation occurred throughout the *Tridacna*'s life (Yan et al., 2020). In general, *Tridacna* A5 grew faster in warm seasons and slower in cold seasons.

The SST observation in the Xisha Islands suggested that the first  $r$  month nearly corresponds to the lowest SST. Thus, the highest  $\delta^{18}\text{O}$  of each cycle was chosen as the beginning of a year.

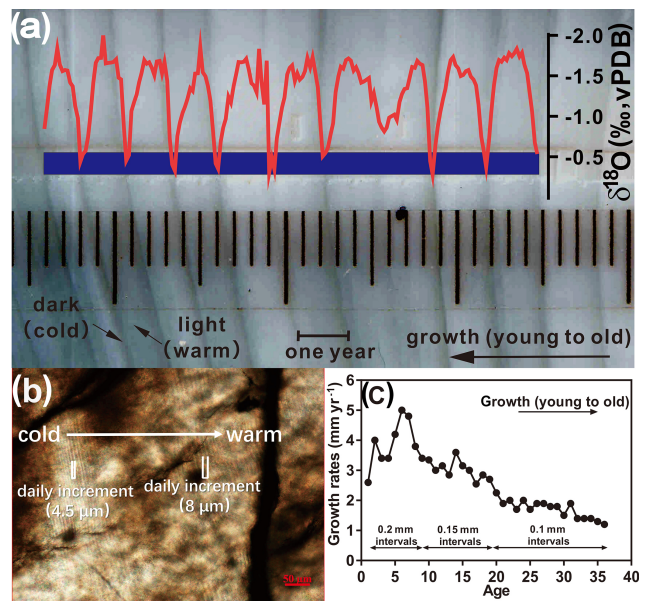


**Figure 3.** (a) Dark–bright lines consistent with  $\delta^{18}\text{O}_{\text{A5}}$  profiles. The blue line represents the sampling line. Dark and bright lines correspond to high  $\delta^{18}\text{O}$  (cold seasons) and low  $\delta^{18}\text{O}$  (warm seasons), respectively. The distance between the dashed lines represents one year, during which the *Tridacna* grew. (b) Under the microscope, daily increments (a dark coupled with a bright increment) are smaller when temperature is cold but larger when temperature is higher. (c) Growth rates (line 2 in Fig. 1c) in fossil *Tridacna* A5.

## 4 Discussion

### 4.1 Relation of SST, SSS, and $\delta^{18}\text{O}$ of modern *Tridacna*

Previous studies have demonstrated that *Tridacna* is in oxygen isotopic equilibrium with the surrounding seawater (Aharon, 1983; Watanabe et al., 1999), which also holds true for *Tridacna* in the South China Sea (Yan et al., 2013). Biogenic carbonate  $\delta^{18}\text{O}$  values show linear correlations with SST and seawater  $\delta^{18}\text{O}_{\text{water}}$  (Aharon and Chappell, 1986; Pätzold et al., 1991; Romanek and Grossman, 1989). The  $\delta^{18}\text{O}_{\text{shell}}-\text{SST}-\delta^{18}\text{O}_{\text{water}}$  Eq. (1) of Grossman and Ku (1986) is adopted, as it is widely used in calculations for tropical aragonite mollusk species. Meanwhile,  $\delta^{18}\text{O}_{\text{water}}$  has a positive relationship with SSS, and Eq. (2), which was established using seawater in the northern South China Sea (Hong et al., 1997), is chosen for the calculation. We merge Eqs. (1) and (2) into  $\delta^{18}\text{O}_{\text{shell}}-\text{SST}-\text{SSS}$  (Eq. 3) to roughly simplify the environmental control on the  $\delta^{18}\text{O}_{\text{shell}}$ .

$$\text{SST} (\text{°C}) = 21.8 - 4.69(\delta^{18}\text{O}_{\text{shell}} - \delta^{18}\text{O}_{\text{water}}) \quad (1)$$

$$\delta^{18}\text{O}_{\text{water}} (\text{\textperthousand}) = 0.23 \times \text{SSS} - 7.58 \quad (2)$$

$$\text{SST} (\text{°C}) = -13.75 - 4.69 \times \delta^{18}\text{O}_{\text{shell}} + 1.08 \times \text{SSS} \quad (3)$$

The  $\delta^{18}\text{O}_{\text{shell}}$  reflects a combination of SST and SSS variation. In order to quantify more precisely the relation between those factors and  $\delta^{18}\text{O}_{\text{shell}}$ , two  $\delta^{18}\text{O}$  profiles are calculated (Fig. 4a):  $\delta^{18}\text{O}_{\text{SST}}$  (constant SSS but varying SST) and  $\delta^{18}\text{O}_{\text{SSS}}$  (constant SST but varying SSS). For the purpose of minimizing the influence of extreme values, mean  $r$ -monthly  $\delta^{18}\text{O}$  profiles ( $\delta^{18}\text{O}_{\text{YX1}}$ ,  $\delta^{18}\text{O}_{\text{SST}}$ , and  $\delta^{18}\text{O}_{\text{SSS}}$ ) are used for the comparison. The results show that  $\delta^{18}\text{O}_{\text{YX1}}$ ,  $\delta^{18}\text{O}_{\text{SST}}$ , and  $\delta^{18}\text{O}_{\text{SSS}}$  profiles are in the range of  $-0.57\text{\textperthousand}$  to  $-1.52\text{\textperthousand}$ ,  $-0.48\text{\textperthousand}$  to  $-1.58\text{\textperthousand}$ , and  $-1.07\text{\textperthousand}$  to  $-1.19\text{\textperthousand}$ , respectively. It is obvious that  $\delta^{18}\text{O}_{\text{YX1}}$  and  $\delta^{18}\text{O}_{\text{SST}}$  show the same trend and are highly correlated ( $r = 0.91$ ,  $n = 7$ ;  $r = 0.78$ ,  $n = 77$ ), but the variation range in  $\delta^{18}\text{O}_{\text{SSS}}$  is only 14 % of  $\delta^{18}\text{O}_{\text{YX1}}$ . Therefore, this indicates that the  $\delta^{18}\text{O}_{\text{shell}}$  in the Xisha Islands corresponds predominantly to seasonal SST variation. In addition, the calculated  $\delta^{18}\text{O}_{\text{predicted}}$  (by using both local actual SST and SSS) was used to compare with  $\delta^{18}\text{O}_{\text{YX1}}$  (Table S1 in the Supplement). The  $\delta^{18}\text{O}_{\text{YX1}}$  and  $\delta^{18}\text{O}_{\text{predicted}}$  profiles have nearly the same mean value ( $1.15\text{\textperthousand}$  and  $1.14\text{\textperthousand}$ , respectively), and their positive correlation ( $r = 0.81$ ,  $n = 77$ ) indicates that the local *Tridacna* precipitates its shell in oxygen isotopic equilibrium.

Moreover, the comparison of predicted SST (under constant SSS and actual SSS with  $\delta^{18}\text{O}_{\text{YX1}}$ ) further confirms that the SSS variation has no significant effect on the local reconstructed SST (Fig. 4f). The two predicted SST values were highly similar ( $r = 0.93$ ), and they are well correlated with the actual SST ( $r_{\text{vary}} = 0.79$ ,  $r_{\text{constant}} = 0.78$ ). Thus, we can use  $\delta^{18}\text{O}_{\text{shell}}$  to roughly estimate the seasonal local SST variation and to establish a new SST– $\delta^{18}\text{O}_{\text{shell}}$  linear regression: SST (°C) =  $22.69 - 4.41 \times \delta^{18}\text{O}_{\text{shell}}$  (or  $\delta^{18}\text{O}_{\text{shell}}$

(\text{\textperthousand}) =  $-0.136 \times \text{SST} + 2.634$ ). A  $1\text{\textperthousand}$  change of  $\delta^{18}\text{O}_{\text{shell}}$  is roughly equal to  $4.41\text{°C}$  of SST. Yu et al. (2005b) summarized many published  $\delta^{18}\text{O}$ –SST slopes for another marine carbonate species, *Porites lutea* coral, and suggested that the slopes could range from  $-0.134$  to  $-0.189$ . Corals from Hainan Island revealed good  $\delta^{18}\text{O}$  vs. SST correlation, with a linear regression slope of  $-0.137$  (Su et al., 2006), very similar to our result ( $-0.136$ ). Consequently, use of the new linear regression for reconstructing the past SST with the fossil  $\delta^{18}\text{O}_{\text{shell}}$  is a valid approach.

### 4.2 Indication of seasonal variation in modern *Tridacna*

According to  $\delta^{18}\text{O}_{\text{YX1}}$  ( $-0.60\text{\textperthousand}$  to  $-1.52\text{\textperthousand}$ ) and  $\delta^{18}\text{O}_{\text{predicted}}$  ( $-0.47\text{\textperthousand}$  to  $-1.57\text{\textperthousand}$ ) profiles (Fig. 4b), seasonality is shown with the lowest value occurring in the first  $r$  month (cold season) and the highest value in the fourth  $r$  month (warm season). The difference in seasonality between  $\delta^{18}\text{O}_{\text{YX1}}$  and  $\delta^{18}\text{O}_{\text{predicted}}$  is  $0.18\text{\textperthousand}$ , which accounts for 19 % of  $\delta^{18}\text{O}_{\text{YX1}}$ . This situation may be due to the different growth rates and equidistance sampling mode. In each year, the analyzed *Tridacna* grew faster in warmer seasons than in colder seasons; thus, specimens under equidistance sampling mode have more samples in the warm seasons. Fewer points in the cold seasons decrease the values and lead to a lower  $\delta^{18}\text{O}_{\text{shell}}$  in the first  $r$  month, but the higher number of points makes  $\delta^{18}\text{O}_{\text{shell}}$  close to  $\delta^{18}\text{O}_{\text{predicted}}$  in the warm seasons (nearly identical in the fourth  $r$  month). Moreover, throughout the life of the analyzed *Tridacna*, the  $\delta^{18}\text{O}_{\text{shell}}$  yearly amplitude increasingly approaches the actual  $\delta^{18}\text{O}_{\text{predicted}}$  when using a greater number of points (fast growth rate) before reaching maturity. After the *Tridacna* reached maturity, the fewer points obtained under equidistance mode in a year yielded a lower amplitude. This can explain the minor discrepancy between  $\delta^{18}\text{O}_{\text{shell}}$  and  $\delta^{18}\text{O}_{\text{predicted}}$ . As a result,  $\delta^{18}\text{O}_{\text{shell}}$  slightly reduced the actual seasonal variation. However, the correlation between them is high ( $r = 0.81$ ,  $n = 77$ ), and the mean  $\delta^{18}\text{O}_{\text{YX1}}$  ( $-1.15\text{\textperthousand}$ ) and mean  $\delta^{18}\text{O}_{\text{predicted}}$  ( $-1.14\text{\textperthousand}$ ) values are similar. Therefore,  $\delta^{18}\text{O}_{\text{shell}}$  can also be used to estimate the actual seasonal variation, with caution regarding the slightly reduced variation.

### 4.3 Reconstructed climate with fossil *Tridacna A5* $\delta^{18}\text{O}$ evidence

The fossil *Tridacna* lived 3700 years ago during the early Meghalayan. The 40  $\delta^{18}\text{O}_{\text{A5}}$  cycles reveal that *Tridacna A5* had probably lived for at least 40 years. After calculating data into  $r$ -monthly average profiles, the extreme seasonal variation effects were minimized. The mean  $\delta^{18}\text{O}_{\text{A5}}$  is  $-1.34\text{\textperthousand}$ , with a minimum and maximum of  $-1.66\text{\textperthousand}$  and  $0.66\text{\textperthousand}$ , respectively (Fig. 4c). Contrasting with the mean value of YX1 ( $-1.15\text{\textperthousand}$ ), the lower  $\delta^{18}\text{O}_{\text{A5}}$  mean value may have reflected the higher temperature that *Tridacna A5* experienced during the warmer season. To translate into SST (without consider-

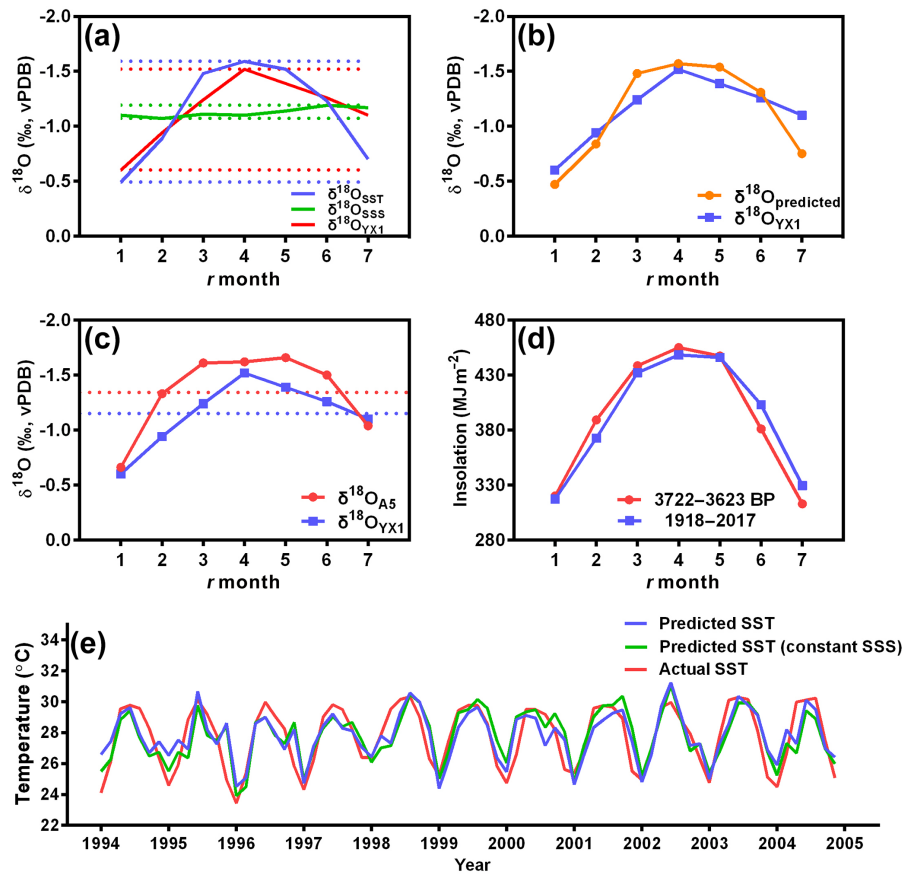


**Figure 4.** (a) Predicted  $r$ -monthly  $\delta^{18}\text{O}$  profiles under constant SSS (blue line) and constant SST (green line) conditions, and  $\delta^{18}\text{O}$  of YX1 (red line). Dotted lines represent the maximum and minimum of the  $r$ -monthly  $\delta^{18}\text{O}$  profiles. (b)  $r$ -monthly  $\delta^{18}\text{O}_{\text{YX1}}$  and  $\delta^{18}\text{O}_{\text{predicted}}$ . The (c)  $r$ -monthly  $\delta^{18}\text{O}_{\text{YX1}}$  and  $\delta^{18}\text{O}_{\text{A5}}$ , and the dotted lines represent mean values. (d) Different insolation 3700 years ago and in the past 100 years. (e) Mean seasonal cycles of reconstructed SST<sub>A5</sub> and North Reef SST. (f) Different SST profiles: predicted SST with varied SSS (blue line), constant SSS (green line), and actual SST (red line), respectively.

ing the SSS changes), the temperature was estimated to be roughly  $0.84^{\circ}\text{C}$  higher than the present. This agrees with other lines of evidence that suggest a higher temperature during that period (Ouyang et al., 2016), considered to be part of the Holocene megathermal in China (Shi et al., 1994).

The average  $r$ -monthly seasonal range of this period (1 ‰) is similar to that yielded from YX1 (0.92 ‰). The SDs of  $\delta^{18}\text{O}_{\text{A5}}$  (0.38 ‰,  $n = 281$ ) and  $\delta^{18}\text{O}_{\text{YX1}}$  (0.35 ‰,  $n = 77$ ) are also similar. These results show similar climate change 3700 years ago and in the present. However, the life of *Tridacna* YX1 (11 years) was much shorter than the fossil *Tridacna* (which lived for at least 40 years), and YX1's location is in the south of A5's location; thus modern observation data from the North Reef were used to do the climatic comparison. After translating  $\delta^{18}\text{O}_{\text{A5}}$  into SST (Fig. 5), the reconstructed SST shows an average maximum and minimum of  $30$  and  $25.61^{\circ}\text{C}$ , respectively, with a seasonal variation of  $4.39^{\circ}\text{C}$  (Fig. 4e). Comparatively, the  $r$ -monthly average range of modern observation is  $29.33$  to  $23.99^{\circ}\text{C}$  (from

1982 to 2017), with a seasonal variation of  $5.34^{\circ}\text{C}$  (Fig. 4e). The warmer climate in the past, associated with seasonality variance, is about  $0.95^{\circ}\text{C}$  lower. Considering the seasonality discrepancy between  $\delta^{18}\text{O}_{\text{shell}}$  and  $\delta^{18}\text{O}_{\text{predicted}}$ , the  $\delta^{18}\text{O}_{\text{shell}}$  has a 19 % lower seasonal variation than  $\delta^{18}\text{O}_{\text{predicted}}$ . Therefore, the actual seasonal variation of A5 (roughly  $5.23^{\circ}\text{C}$ ) is still below present seasonality.

In addition, the discrepancy between mean  $\delta^{18}\text{O}_{\text{A5}}$  and mean  $\delta^{18}\text{O}_{\text{YX1}}$  is  $0.19$  ‰; the lower mean  $\delta^{18}\text{O}_{\text{A5}}$  is because of more  $r$  months in lower values. This reveals a possible prolonged high-temperature period 3700 years ago: warm seasons may have been longer, while cold seasons may have been shorter. This agrees with a comparison between 3700 years ago (3722 to 3623 BP) and the past century (1918 to 2017), which indicates *Tridacna* A5 lived in more insolation. This occurs from the second to fifth  $r$  month (warm seasons); however, less insolation occurs in the rest of the months (Fig. 4d). Thus, the prolonged high temperature in the past might be attributed to more insolation. In

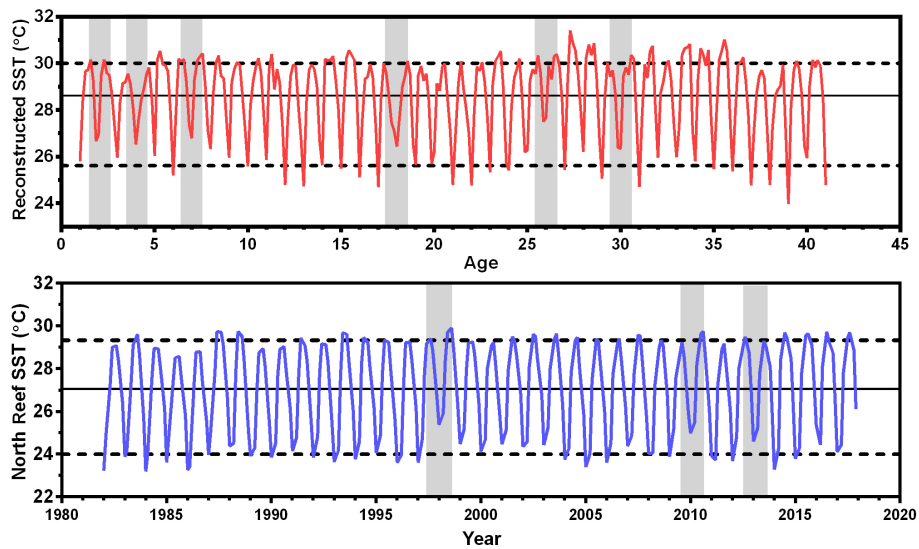


**Figure 5.** Reconstructed SST around 3700 years ago (red), compared with the North Reef SST from 1982 to 2017 (blue). Dotted lines represent the average maximum and minimum SST. The gray field represents extreme El Niño winter events.

addition, although a higher sampling density obtained in the warm seasons enlarges the high-temperature period (from the second to sixth  $r$  month), a cold-to-warm transition could still be recognized in A5 and YX1  $\delta^{18}\text{O}$  profiles (Fig. 4c). Comparison of each  $r$ -monthly value with the average value shows that between the first and second  $r$  month, there was a larger deviation with a greater slope 3700 years ago. This illustrates a fast transition between cold and warm seasons 3700 years ago. As  $\delta^{18}\text{O}_{\text{predicted}}$  has stronger seasonal variation than  $\delta^{18}\text{O}_{\text{shell}}$ , the slope should be sharper, which means more significant actual seasonal transition.

Overall, the climate around 3700 years ago had slightly lower seasonality than the present, and the transition between cold and warm seasons was starker.

#### 4.4 Climate variation comparison between 3700 years ago and present

A comparison was performed between the modern instrumental observations (from 1982 to 2017) in the North Reef and the reconstructed SST anomalies of *Tridacna* A5. The  $r$ -monthly resolution data were first compared, obtained by subtracting the  $r$ -monthly SST with the mean value of each  $r$  month. In terms of long-term climatic variation, the SST anomalies are markedly different between the 36-year modern instrumental data and the 40-year reconstructed data (Fig. 6a). The SST anomalies (3700 years ago) have sharper peaks and a greater amplitude than in those of recent years, and the SD in the past is much larger (0.68  $^{\circ}\text{C}$ ) than in the present (0.42  $^{\circ}\text{C}$ ), suggesting more severe climate conditions in the past. However, the deviation should be noted alongside the different growth rates during *Tridacna*'s life span and in equidistant sampling mode. For example, *Tridacna*

may have different annual growth rates; hence an  $r$ -monthly value may not represent the corresponding actual  $r$ -monthly value under equidistant sampling mode. In this respect, the  $r$ -annual SST anomalies are estimated to reduce the deviation (Fig. 6b). The SD of modern observation SST anomalies is 0.30  $^{\circ}\text{C}$ , and the SD of reconstructed SST anomalies is 0.41  $^{\circ}\text{C}$ . This illustrates that the modern-to-past ratios of the  $r$ -monthly resolutions or  $r$ -annual resolutions are almost the same (0.65 and 0.73, respectively); thus the SD of  $r$ -monthly SST anomalies of *Tridacna* is likely a reliable measure. As a result, the enhanced climate variability 3700 years ago probably indicates increased ENSO-related variability in this region. This conclusion contradicts data from samples (deep-sea sediments and fossil mollusk shells) collected in the eastern tropical Pacific at the same time period (Koutavas et al., 2012, Carré et al., 2014). More data should be analyzed from long, successive time periods to understand more about the dynamics of ENSO on a large scale.

#### 4.5 ENSO activity recorded by *Tridacna* $\delta^{18}\text{O}$

As ENSO is the strongest contributor to global interannual climate variation, a better understanding of its fundamental properties will allow us to better unravel past climate change episodes and to make more accurate predictions for the future. Interannual climate changes in the Xisha Islands were likely dominated by ENSO activity. The local accumulated positive percentage of monthly SST anomaly threshold responds to 76.47 % El Niño and 79.41 % La Niña events in the Ninō 3.4 region (Liu et al., 2016). Previous studies demonstrate that marine biogenic carbonate-based SST reconstructions in the northern South China Sea likely responded to ENSO activity (Sun et al., 2005; Yan et al., 2017). Warm

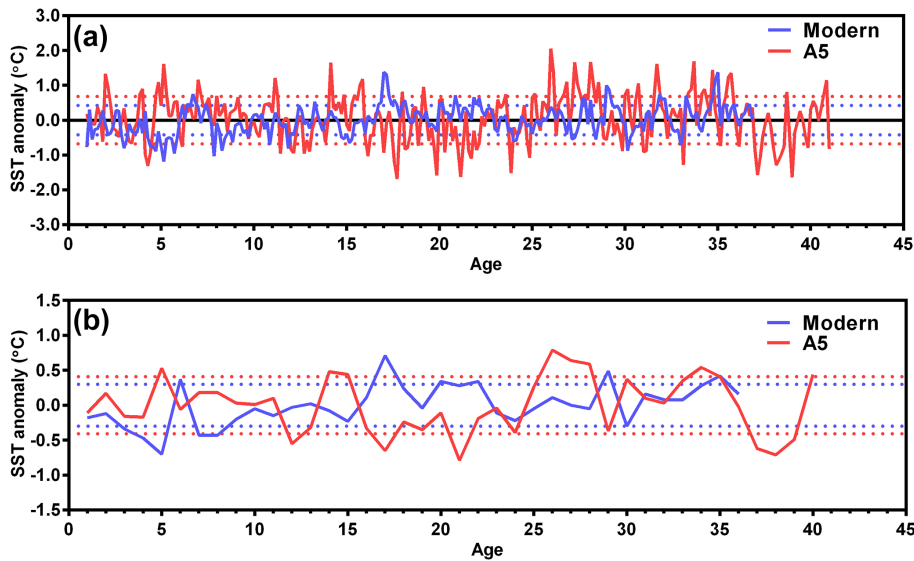


**Figure 6.** SST anomalies of modern instrumental data and reconstructed SST anomalies of *Tridacna* A5 under *r*-monthly (**a**) and *r*-annual (**b**) resolution. Dotted lines represent a standard deviation ( $1\sigma$ ) of SST anomalies.

(cold) SST anomalies are related to El Niño (La Niña) events. Coral has one of the earliest records revealing ENSO events (Peng et al., 2003; Sun et al., 2005; Wei et al., 2007), yet there are still some technical limitations in using coral, such as those concerning post-depositional diagenetic alteration between aragonite and calcite (McGregor and Gagan, 2003). Analyses of *Tridacna* species are performed to overcome this limitation by taking advantage of their denser shells, lack of diagenetic alteration, and oxygen isotopic equilibrium with seawater. Recently, Yan et al. (2014) proved that *Tridacna* species in the Xisha Islands respond to ENSO activity, and then they used fossil *Tridacna*  $\delta^{18}\text{O}$  on Dongdao Island (part of the Xisha Islands) to reconstruct the ENSO variability around 2000 years ago (Yan et al., 2017).

To acquire more precise ENSO reconstructions, modern observation data were analyzed and compared with the SST in Ninó 1 + 2 region. The SST anomaly series were calculated by subtracting the *r*-monthly mean values. The spectral analyses were performed to test periodicity among all SST anomalies (Fig. 7), which indicate a spectral peak of 3 to 7 years. According to the SST series, the North Reef SST has a 3-*r*-month time lag behind the Ninó 1 + 2 SST (Fig. 8a), and thus 3 *r* months of the North Reef SST were brought forward to eliminate the lag. To reconstruct the occurrence of ENSO in the North Reef, 3–7 years of bandpass filtering was performed on the SST anomalies, which yielded North Reef ENSO activity mostly consistent with the Ninó 1 + 2 SST anomalies (Fig. 8c). A threshold value was calculated under  $1\sigma$  SST anomalies for moderate El Niño–La Niña events. A total of 7 El Niño and 10 La Niña events occurred in the past 36 years. In other words, El Niño–La Niña events occurred successively at a 5.14-year frequency in the North Reef.

Spectral analysis revealed that  $\delta^{18}\text{O}_{\text{A}5}$  anomalies also have a 3–7-year period (Fig. 7c). As discussed above, the *Tridacna*  $\delta^{18}\text{O}$  values are mainly dominated by SST in the Xisha Islands, and  $1\text{\textperthousand } \delta^{18}\text{O}_{\text{shell}}$  is roughly equal to  $4.41\text{ }^{\circ}\text{C}$  of SST.  $\delta^{18}\text{O}_{\text{A}5}$  anomalies were transformed into the North Reef SST<sub>A5</sub> anomalies (Fig. 9b). After the 3–7 years of bandpass filtering of the North Reef SST<sub>A5</sub> anomalies, six El Niño and five La Niña events were estimated to occur over 40 years with a  $1\sigma$  SST<sub>A5</sub> anomaly threshold (Fig. 9c), giving a 6.67- and 8-year frequency, respectively. The ENSO frequency is reduced when compared with modern observation data. The lower frequency is supported in ENSO reconstructions back to 7 ka, which suggest a notable reduction of ENSO between 5 and 3 ka (Liu et al., 2013; McGregor et al., 2013; Tudhope et al., 2001; Emile-Geay et al., 2016). However, implications drawn from a mere 40-year-long *Tridacna*  $\delta^{18}\text{O}$  record are likely inconclusive. A collection of more similar-aged *Tridacna* is needed to develop a more continuous climate and ENSO activity record in Holocene.

#### 4.6 Extreme winter El Niño records in fossil *Tridacna* $\delta^{18}\text{O}$ values

In recent decades, extreme El Niño has brought about many climatic disasters, such as catastrophic flooding, bushfire and drought (Ramírez and Briones, 2017; Staupe-Delgado et al., 2018; Yu et al., 2018, 2019). With global warming persisting, the question of whether high temperatures are related to extreme El Niño events is still controversial. Therefore, records of extreme El Niño events in past warm periods are important. Here, the winter SST is used to estimate extreme El Niño events. Winters in the northern South China Sea are very dry, and the SSS variation caused by rainfall is small.

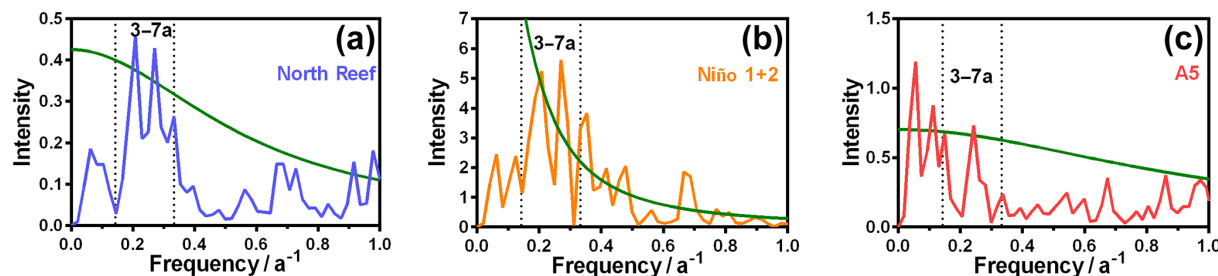


**Figure 7.** Spectral analysis of the North Reef SST anomalies (a), Niño 1 + 2 SST anomalies (b), and reconstructed SST anomalies according to  $\delta^{18}\text{O}_{\text{A}5}$  (c). Green lines indicate significance at the 90 % confidence level, and the area between the two dotted lines represents the frequency of 3 to 7 years.

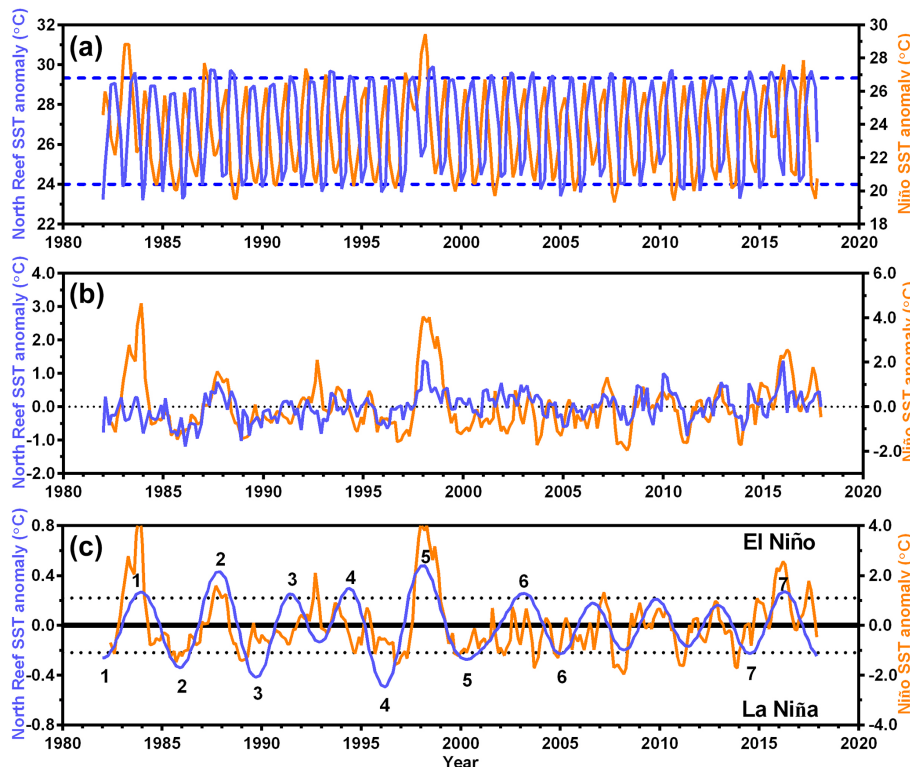


**Figure 8.** Relationship between Niño 1 + 2 SST and the North Reef SST: (a) the North Reef SST (blue line) compared with Niño 1 + 2 SST (yellow line); a clear time lag exists. (b) SST anomalies of two areas; the lag is removed by forwarding the North Reef SST anomalies for 3 months. (c) The North Reef SST anomalies were performed with 3–7 years of bandpass filtering, consistent with Niño 1 + 2 SST anomalies; the dashed lines show the calculated threshold limits ( $1\sigma$ ) for ENSO activity in the North Reef. El Niño and La Niña events are represented by positive and negative SST anomaly values, respectively.

Thus, the SST determined from  $\delta^{18}\text{O}_{\text{shell}}$  should be close to the actual value. The SST calculated by  $\delta^{18}\text{O}_{\text{YX1}}$  reveals a warmer winter in 1998, corresponding to a stronger El Niño that year. A comparison between the reconstructed SST (calculated with  $\delta^{18}\text{O}_{\text{A}5}$ ) and modern observation data from the North Reef (Fig. 5) suggested that the average winter SST 3700 years ago was 25.62 °C. There are six distinctly high SSTs within the 40 years (gray fields in Fig. 5), with anomalies ranging from 0.73 to 2.00 °C. As for the SST of modern observations (from 1982 to 2017), the average of winter SST

is 23.99 °C, and three anomalously warm temperatures vary from 0.60 to 1.38 °C. It seems that extreme El Niño winter events were very frequent in this past warm period. However, this analysis still provides low confidence in answering this controversial question about the relationship between El Niño events and warm climate; more *Tridacna* in the past warm period should be analyzed in future work. Nevertheless, our results still put forward high-resolution data that make a contribution to future work on how El Niño events occur in warm periods.

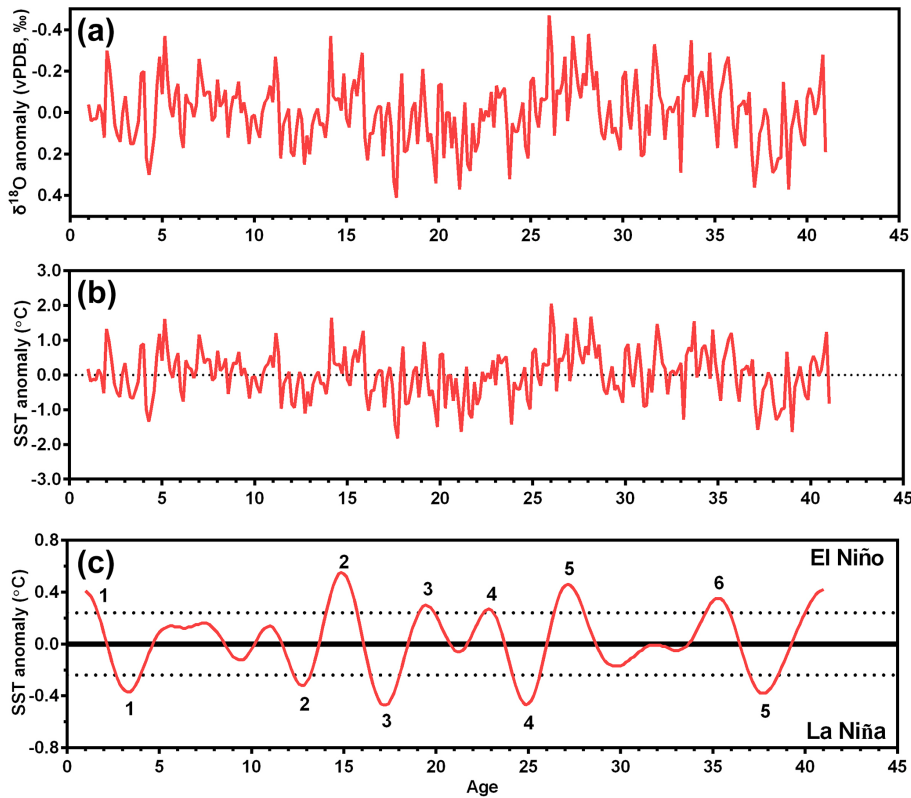


**Figure 9.** (a) ENSO activity reconstructed by the fossil *Tridacna* 3700 years ago:  $\delta^{18}\text{O}$  anomalies of fossil *Tridacna* A5. (b) The North Reef SST anomalies calculated by  $\delta^{18}\text{O}$  anomalies, based on modern *Tridacna*  $\delta^{18}\text{O}$ -SST equation ( $1\text{‰ } \delta^{18}\text{O}_{\text{shell}} \approx 4.41\text{ °C SST}$ ). (c) ENSO activity according to the North Reef SST anomalies after 3–7 years of bandpass filtering; the dashed lines show the calculated threshold limits ( $1\sigma$ ) for ENSO activity.

## 5 Conclusions

The  $\delta^{18}\text{O}$  values derived from *Tridacna* provide high-resolution data, useful to unravel climatic variability and ENSO activity. In the Xisha Islands of the northern South China Sea, the  $\delta^{18}\text{O}_{\text{shell}}$  of modern *Tridacna gigas* can serve as a proxy for SST, while SSS has a minor effect on the  $\delta^{18}\text{O}_{\text{shell}}$ . Thus, a rough  $\delta^{18}\text{O}$ -SST linear regression is established:  $\text{SST } (\text{°C}) = 22.69 - 4.41 \times \delta^{18}\text{O}_{\text{shell}}$ . Another *Tridacna squamosa* A5, which lived 3700 years ago, reveals 40 clearly dark–bright line couples consistent with  $\delta^{18}\text{O}_{\text{shell}}$  profiles. Reconstructed SST implies a warmer climate 3700 years ago,  $0.84\text{ °C}$  higher than the present. The seasonal variation slightly decreased, and the transition among cold to warm seasons was faster. The combinations of SST anomalies reconstructed at  $r$ -monthly– $r$ -annual resolution suggest enhanced ENSO-related variability during this past warm period. In addition, the frequency of ENSO activity was less 3700 years ago than during the recent 36 years of modern observations. El Niño–La Niña events occurred alternatively at a frequency of every 6.67 and 8 years in the past, compared to every 5.14 years in recent decades. Extreme El Niño winters have been recorded by a fossil *Tridacna* with

increased numbers and intense variations. Our results imply an unstable climate 3700 years ago, although more data are still needed to support this hypothesis.

**Data availability.** All data can be acquired in the Supplement. Some of meteorological data are deposited at the NOAA website (<http://www.cpc.ncep.noaa.gov/data/indices/sstoi.indices>, last access: 31 December 2017). The dating result of *Tridacna* is calibrated by CALIB 7.10 Radiocarbon Calibration (<http://calib.org>, Stuiver et al., 2018). Correspondence and requests for materials should be addressed to Xiaoming Sun (eessxm@mail.sysu.edu.cn) and Hong Yan (yanhong@ieecas.cn).

**Supplement.** The supplement related to this article is available online at: <https://doi.org/10.5194/cp-16-597-2020-supplement>.

**Author contributions.** XS, HY, and YH designed the research and experiments; HY collected the samples; HC and YH performed stable isotope measurements. HY and YH did the data analyses. YH wrote the manuscript, with the help of all co-authors.

**Competing interests.** The authors declare that they have no conflict of interest.

**Acknowledgements.** We are grateful to Yu Fu, Yang Lu, Jiaoyang Ruan, Chengcheng Liu, Tianjian Yang, and Jun Gu for their support in preparing the manuscript. Youfeng Ning, Hanying Li, Pengfei Duan, and Jingyao Zhao are thanked for their technical support in drilling and analyses at Xi'an Jiaotong University.

**Financial support.** This research has been supported by the National Key R&D Program of China (2018YFA0702605), the National 13th Five Year Plan project (DY135-R2-1-01, DY135-C1-1-06), National Nature Science Foundation of China (41876038, 41877399, 91128101, 41888101), State Key Laboratory for Mineral Deposits Research in Nanjing University (no. 20-15-07), Chinese Academy of Sciences (QYZDB-SSW-DQC001), and the Qingdao National Laboratory for Marine Science and Technology of China (QNL2016ORP0202).

**Review statement.** This paper was edited by Denis-Didier Rousseau and reviewed by two anonymous referees.

## References

- Agbaje, O. B. A., Wirth, R., Morales, L. F. G., Shirai, K., Kosnik, M., Watanabe, T., and Jacob, D. E.: Subject Category: Subject Areas: Architecture of crossed-lamellar bivalve shells: the southern giant clam (*Tridacna derasa*, Röding, 1798), R. Soc. Open Sci., 4, 1–15, <https://doi.org/10.1098/rsos.170622>, 2017.
- Aharon, P.: 140,000-yr isotope climatic record from raised coral reefs in New Guinea, Nature, 304, 720–723, <https://doi.org/10.1038/304720a0>, 1983.
- Aharon, P.: Recorders of reef environment histories: stable isotopes in corals, giant clams, and calcareous algae, Coral Reefs, 10, 71–90, <https://doi.org/10.1007/BF00571826>, 1991.
- Aharon, P. and Chappell, J.: Oxygen isotopes, sea level changes and the temperature history of a coral reef environment in New Guinea over the last 105 years, Palaeogeogr. Palaeoecol., 56, 337–379, [https://doi.org/10.1016/0031-0182\(86\)90101-X](https://doi.org/10.1016/0031-0182(86)90101-X), 1986.
- Arias-Ruiz, C., Elliot, M., Bézos, A., Pedoja, K., Husson, L., Cahyarini, S. Y., Cariou, E., Michel, E., La, C., and Manssouri, F.: Geochemical fingerprints of climate variation and the extreme La Niña 2010–11 as recorded in a *Tridacna squamosa* shell from Sulawesi, Indonesia, Palaeogeogr. Palaeoecol., 487, 216–228, <https://doi.org/10.1016/j.palaeo.2017.08.037>, 2017.
- Ayling, B. F., Chappell, J., Gagan, M. K., and McCulloch, M. T.: ENSO variability during MIS 11 (424–374 ka) from *Tridacna gigas* at Huon Peninsula, Papua New Guinea, Earth Planet. Sc. Lett., 431, 236–246, <https://doi.org/10.1016/j.epsl.2015.09.037>, 2015.
- Batenburg, S. J., Reichart, G. J., Jilbert, T., Janse, M., Wesselingh, F. P., and Renema, W.: Interannual climate variability in the Miocene: High resolution trace element and stable isotope ratios in giant clams, Palaeogeogr. Palaeoecol., 306, 75–81, <https://doi.org/10.1016/j.palaeo.2011.03.031>, 2011.
- Cane, M. A.: The evolution of El Niño, past and future, Earth Planet. Sc. Lett., 230, 227–240, <https://doi.org/10.1016/j.epsl.2004.12.003>, 2005.
- Carré, M., Sachs, J. P., Purca, S., Schauer, A. J., Braconnot, P., Falcón, R. A., Julien, M., and Lavallée, D.: Holocene history of ENSO variance and asymmetry in the eastern tropical Pacific, Paleoceanography, 345, 1045–1048, <https://doi.org/10.1126/science.1252220>, 2014.
- Cobb, K. M., Westphal, N., Sayani, H. R., Watson, J. T., Lorenzo, E. Di, Cheng, H., Edwards, R. L., and Charles, C. D.: Highly Variable El Niño–Southern Oscillation Throughout the Holocene, Science, 339, 67–70, <https://doi.org/10.1126/science.1228246>, 2014.
- Duprey, N., Galipaud, J. C., Cabioch, G., and Lazareth, C. E.: Isotopic records from archeological giant clams reveal a variable climate during the southwestern Pacific colonization ca. 3.0ka BP, Palaeogeogr. Palaeoecol., 404, 97–108, <https://doi.org/10.1016/j.palaeo.2014.04.002>, 2014.
- Elliot, M., Welsh, K., Chilcott, C., McCulloch, M., Chappell, J., and Ayling, B.: Profiles of trace elements and stable isotopes derived from giant long-lived *Tridacna gigas* bivalves: Potential applications in paleoclimate studies, Palaeogeogr. Palaeoecol., 280, 132–142, <https://doi.org/10.1016/j.palaeo.2009.06.007>, 2009.
- Emile-Geay, J., Cobb, K. M., Carre, M., Braconnot, P., Leloup, J., Zhou, Y., Harrison, S. P., Corrège, T., McGregor, H. V., Collins, M., Driscoll, R., Elliot, M., Schneider, B., and Tudhope, A.: Links between tropical Pacific seasonal, interannual and orbital variability during the Holocene, Nat. Geosci., 9, 168–173, <https://doi.org/10.1038/ngeo2608>, 2016.
- Gannon, M. E., Pérez-Huerta, A., Aharon, P., and Street, S. C.: A biomineralization study of the Indo-Pacific giant clam *Tridacna gigas*, Coral Reefs, 36, 503–517, <https://doi.org/10.1007/s00338-016-1538-5>, 2017.
- Grossman, E. L. and Ku, T. L.: Oxygen and carbon isotope fractionation in biogenic aragonite: Temperature effects, Chem. Geol., 59, 59–74, [https://doi.org/10.1016/0016-9622\(86\)90057-6](https://doi.org/10.1016/0016-9622(86)90057-6), 1986.
- Hong, A., Hong, Y., Wang, Q., and Ke, J.: Distributive characteristics of O isotope of the northeastern South China Sea in the summer of 1994, Trop. Oceanol., 16, 82–90, 1997.
- Koutavas, A. and Joanides, S.: El Niño – Southern Oscillation extrema in the Holocene and Last Glacial Maximum, Paleoceanography, 27, 1–15, <https://doi.org/10.1029/2012PA002378>, 2012.
- Laskar, J., Robutel, P., Joutel, F., Gastineau, M., Correia, A. C. M., and Levrard, B.: A long-term numerical solution for the insolation quantities of the Earth, Astron. Astrophys., 428, 261–285, <https://doi.org/10.1051/0004-6361:20041335>, 2004.
- Liu, C., Yan, H., Fei, H., Ma, X., Zhang, W., and Shi, G.: Journal of Asian Earth Sciences Temperature seasonality and ENSO variability in the northern South China Sea during the Medieval Climate Anomaly interval derived from the Sr/Ca ratios of *Tridacna* shell, J. Asian Earth Sci., 180, 1–9, <https://doi.org/10.1016/j.jseas.2019.103880>, 2019.
- Liu, C., Zhang, W., and Yan, H.: Relationship between El Niño–Southern Oscillation events and regional sea surface temperature anomalies around the Xisha Islands, South China Sea, J. Earth Environ., 1, 1188–1197, <https://doi.org/10.7515/JEE201702007>, 2016.

- Liu, C., Yan, H., Fei, H., Ma, X., Zhang, W., and Shi, G.: Journal of Asian Earth Sciences Temperature seasonality and ENSO variability in the northern South China Sea during the Medieval Climate Anomaly interval derived from the Sr/Ca ratios of *Tridacna* shell, *J. Asian Earth Sci.*, 180, 1–9, <https://doi.org/10.1016/j.jseas.2019.103880>, 2019.
- Liu, J., Li, T., Xiang, R., Chen, M., Yan, W., Chen, Z., and Liu, F.: Influence of the Kuroshio Current intrusion on Holocene environmental transformation in the South China Sea, *Holocene*, 23, 850–859, <https://doi.org/10.1177/0959683612474481>, 2013.
- McGregor, H. V. and Gagan, M. K.: Diagenesis and geochemistry of Porites corals from Papua New Guinea: Implications for paleoclimate reconstruction, *Geochim. Cosmochim. Ac.*, 67, 2147–2156, [https://doi.org/10.1007/430\\_2015\\_174](https://doi.org/10.1007/430_2015_174), 2003.
- McGregor, H. V., Fischer, M. J., Gagan, M. K., Fink, D., Phipps, S. J., Wong, H., and Woodroffe, C. D.: A weak El Niño/Southern Oscillation with delayed seasonal growth around 4,300 years ago, *Nat. Geosci.*, 6, 949–953, <https://doi.org/10.1038/ngeo1936>, 2013.
- Mitsuguchi, T., Dang, P. X., Kitagawa, H., Uchida, T., and Shiba, Y.: Coral Sr/Ca and Mg/Ca records in Con Dao Island off the Mekong Delta: Assessment of their potential for monitoring ENSO and East Asian monsoon, *Global Planet. Change*, 63, 341–352, <https://doi.org/10.1016/j.gloplacha.2008.08.002>, 2008.
- Ourbak, T., Corrège, T., Malaizé, B., Le Correc, F., Charlier, K., and Peypouquet, J. P.: ENSO and interdecadal climate variability over the last century documented by geochemical records of two coral cores from the South West Pacific, *Adv. Geosci.*, 6, 23–27, <https://doi.org/10.5194/adgeo-6-23-2006>, 2006.
- Ouyang, T., Li, M., Zhao, X., Zhu, Z., Tian, C., Qiu, Y., Peng, X., and Hu, Q.: Sensitivity of Sediment Magnetic Records to Climate Change during Holocene for the Northern South China Sea, *Front. Earth Sci.*, 4, 1–12, <https://doi.org/10.3389/feart.2016.00054>, 2016.
- Pätzold, J., Heinrichs, J. P., Wolschendorf, K., and Wefer, G.: Correlation of stable oxygen isotope temperature record with light attenuation profiles in reef-dwelling *Tridacna* shells, *Coral Reefs*, 10, 65–69, <https://doi.org/10.1007/BF00571825>, 1991.
- Peng, Z., Chen, T., Nie, B., Head, M. J., He, X., and Zhou, W.: Coral  $\delta^{18}\text{O}$  records as an indicator of winter monsoon intensity in the South China Sea, *Quaternary Res.*, 59, 258–292, [https://doi.org/10.1016/S0033-5894\(03\)00042-5](https://doi.org/10.1016/S0033-5894(03)00042-5), 2003.
- Ramírez, I. J. and Briones, F.: Understanding the El Niño Costero of 2017: The Definition Problem and Challenges of Climate Forecasting and Disaster Responses, *Int. J. Disast. Risk Sci.*, 8, 489–492, <https://doi.org/10.1007/s13753-017-0151-8>, 2017.
- Rodbell, D. T., Seltzer, G. O., Anderson, D. M., Abbott, M. B., Enfield, D. B., and Newman, J. H.: An  $\sim 15\text{000}$ -Year Record of El Niño-Driven Alluviation in Southwestern Ecuador.pdf, *Science*, 283, 516–520, <https://doi.org/10.1126/science.283.5401.516>, 1999.
- Romanek, C. S. and Grossman, E. L.: Stable Isotope Profiles of *Tridacna* maxima as Environmental Indicators Stable Isotope Profiles of *Tridacna* maxima as Environmental Indicators, *Palaios*, 4, 402–413, <https://doi.org/10.2307/351458>, 1989.
- Schirrmacher, J., Weinelt, M., Blanz, T., Andersen, N., Salgueiro, E., and Schneider, R. R.: Multi-decadal climate variability in southern Iberia during the mid- to late-Holocene, *Clim. Past*, 15, 617–634, <https://doi.org/10.5194/cp-15-367-2019>, 2019.
- Schöne, B. R. and Fiebig, J.: Seasonality in the North Sea during the Allerød and Late Medieval Climate Optimum using bivalve sclerochronology, *Int. J. Earth Sci.*, 98, 83–98, <https://doi.org/10.1007/s00531-008-0363-7>, 2009.
- Schöne, B. R., Fiebig, J., Pfeiffer, M., Gleß, R., Hickson, J., Johnson, A. L. A., Dreyer, W., and Oschmann, W.: Climate records from a bivalved Methuselah (*Arctica islandica*, Mollusca; Iceland), *Palaeogeogr. Palaeoclimatol. Palaeoecol.*, 228, 130–148, <https://doi.org/10.1016/j.palaeo.2005.03.049>, 2005.
- Schöne, B. R., Fiebig, J., Pfeiffer, M., Gleß, R., Hickson, J., Johnson, A. L. A., Dreyer, W., and Oschmann, W.: Climate records from a bivalved Methuselah (*Arctica islandica*, Mollusca; Iceland), *Palaeogeogr. Palaeoclimatol. Palaeoecol.*, 228, 130–148, <https://doi.org/10.1016/j.palaeo.2005.03.049>, 2005.
- Scuderi, L. A., Yang, X., Ascoli, S. E., and Li, H.: The 4.2 ka BP Event in northeastern China: a geospatial perspective, *Clim. Past*, 15, 367–375, <https://doi.org/10.5194/cp-15-367-2019>, 2019.
- Shi, Y., Kong, Z., Wang, S., Tang, L., Wang, F., Yao, T., Zhao, X., Zhang, P., and Shi, S.: The Climatic Fluctuation and Important Events of Holocene Megathermal in China, *Sci. China*, 3, 353–365,, 1994.
- Staude-Delgado, R., Kruke, B. I., Ross, R. J., and Glantz, M. H.: Preparedness for slow-onset environmental disasters: Drawing lessons from three decades of El Niño impacts, *Sustain. Dev.*, 26, 553–563, <https://doi.org/10.1002/sd.1719>, 2018.
- Stuiver, M., Reimer, P. J., and Reimer, R. W.: available at: <http://calib.org>, last access: 31 December 2018.
- Su, R., Sun, D., Bloemendal, J., and Zhu, Z.: Temporal and spatial variability of the oxygen isotopic composition of massive corals from the South China Sea: Influence of the Asian monsoon, *Palaeogeogr. Palaeoclimatol. Palaeoecol.*, 240, 630–648, <https://doi.org/10.1016/j.palaeo.2006.03.012>, 2006.
- Sun, D., Gagan, M. K., Cheng, H., Scott-Gagan, H., Dykoski, C. A., Edwards, R. L., and Su, R.: Seasonal and interannual variability of the Mid-Holocene East Asian monsoon in coral  $\delta^{18}\text{O}$  records from the South China Sea, *Earth Planet. Sc. Lett.*, 237, 69–84, <https://doi.org/10.1016/j.epsl.2005.06.022>, 2005.
- Thompson, L. G., Davis, M. E., Lin, P., Henderson, K. A., Bolzan, J. F., and Liu, K.: Late glacial stage and Holocene tropical ice core records from Huascarán, Peru, *Science*, 269, 46–50, <https://doi.org/10.1126/science.269.5220.46>, 1995.
- Toth, L. T. and Aronson, R. B.: The 4.2 ka event, ENSO, and coral reef development, *Clim. Past*, 15, 105–119, <https://doi.org/10.5194/cp-15-105-2019>, 2019.
- Tudhope, A. W., Chilcott, C. P., McCulloch, M. T., Cook, E. R., Chappell, J., Ellam, R. M., W. Lea, D., Lough, J. M., and Shimield, G. B.: Variability in the El Niño-Southern Oscillation through a glacial-interglacial cycle, *Science*, 291, 1511–1517, <https://doi.org/10.1126/science.1057969>, 2001.
- Wanamaker, A. D., Kreutz, K. J., Schöne, B. R., and Introne, D. S.: Gulf of Maine shells reveal changes in seawater temperature seasonality during the Medieval Climate Anomaly and the Little Ice Age, *Palaeogeogr. Palaeoclimatol. Palaeoecol.*, 302, 43–51, <https://doi.org/10.1016/j.palaeo.2010.06.005>, 2011.
- Watanabe, T., Oba, T., and Dee, V.: Daily reconstruction of water temperature from oxygen isotopic ratios of a modern *Tridacna* shell using a freezing microtome sampling technique was recorded monthly to seasonal sea surface to reconstruct using Jones maturity of *Tridacna max-*

- ima* resolution f, J. Geophys. Res., 104, 20667–20674, <https://doi.org/10.1029/1999JC900097>, 1999.
- Watanabe, T., Suzuki, A., Kawahata, H., Kan, H., and Ogawa, S.: A 60-year isotopic record from a mid-Holocene fossil giant clam (*Tridacna gigas*) in the Ryukyu Islands: Physiological and paleoclimatic implications, Palaeogeogr. Palaeoecol., 212, 343–354, <https://doi.org/10.1016/j.palaeo.2004.07.001>, 2004.
- Wei, G., Deng, W., Yu, K., Li, X. H., Sun, W., and Zhao, J. X.: Sea surface temperature records in the northern South China Sea from mid-Holocene coral Sr/Ca ratios, Paleoceanography, 22, 1–13, <https://doi.org/10.1029/2006PA001270>, 2007.
- Welsh, K., Elliot, M., Tudhope, A., Ayling, B., and Chappell, J.: Giant bivalves (*Tridacna gigas*) as recorders of ENSO variability, Earth Planet. Sc. Lett., 307, 266–270, <https://doi.org/10.1016/j.epsl.2011.05.032>, 2011.
- Woodroffe, C. D., Beech, M. R., and Gagan, M. K.: Mid-late Holocene El Niño variability in the equatorial Pacific from coral microatolls, Geophys. Res. Lett., 30, 1–4, <https://doi.org/10.1029/2002GL015868>, 2003.
- Yamanashi, J., Takayanagi, H., Isaji, A., Asami, R., and Iryu, Y.: Carbon and oxygen isotope records from *Tridacna derasa* shells: Toward establishing a reliable proxy for sea surface environments, PLoS One, 11, 1–19, <https://doi.org/10.1371/journal.pone.0157659>, 2016.
- Yan, H., Sun, L., Liu, X., and Qiu, S.: Relationship between ENSO events and regional climate anomalies around the Xisha Islands during the last 50 years, J. Trop. Oceanogr., 29, 29–35, <https://doi.org/10.1007/s13131-014-0399-4>, 2010.
- Yan, H., Shao, D., Wang, Y., and Sun, L.: Sr/Ca profile of long-lived *Tridacna gigas* bivalves from South China Sea: A new high-resolution SST proxy, Geochim. Cosmochim. Ac., 112, 52–65, <https://doi.org/10.1016/j.gca.2013.03.007>, 2013.
- Yan, H., Wang, Y., and Sun, L.: High resolution oxygen isotope and grayscale records of a medieval fossil giant clam (*Tridacna gigas*) in the South China Sea: Physiological and paleoclimatic implications, Acta Oceanol. Sin., 33, 18–25, <https://doi.org/10.1007/s13131-014-0399-4>, 2014.
- Yan, H., Liu, C., Zhang, W., Li, M., Zheng, X., Wei, G., Xie, L., Deng, W., and Sun, L.: ENSO variability around 2000 years ago recorded by *Tridacna gigas*  $\delta^{18}\text{O}$  from the South China Sea, Quatern. Int., 452, 148–154, <https://doi.org/10.1016/j.quaint.2016.05.011>, 2017.
- Yan, H., Liu, C., An, Z., Yang, W., Yang, Y., Huang, P., Qiu, S., Zhou, P., Zhao, N., Fei, H., Ma, X., Shi, G., Dodson, J., Hao, J., Yu, K., Wei, G., Yang, Y., Jin, Z., and Zhou, W.: Extreme weather events recorded by daily to hourly resolution biogeochemical proxies of marine Giant Clam shells, P. Natl. Acad. Sci. USA, 1–6, <https://doi.org/10.1073/pnas.1916784117>, 2020.
- Yang, Y., Xiang, R., Liu, J., and Tang, L.: Inconsistent sea surface temperature and salinity changing trend in the northern South China Sea since 7.0 ka BP, J. Asian Earth Sci., 171, 178–186, <https://doi.org/10.1016/j.jseaes.2018.05.033>, 2019.
- Yu, J., Qi, M., Sun, Q., and Tao, L.: Statistical characteristics of summer extreme rainfall over eastern China and its relation with El Niño, J. Nanjing Inst. Meteorol., 41, 77–84, 2018.
- Yu, K. F., Zhao, J. X., Wei, G. J., Cheng, X. R., and Wang, P. X.: Mid-late Holocene monsoon climate retrieved from seasonal Sr/Ca and  $\delta^{18}\text{O}$  records of *Porites lutea* corals at Leizhou Peninsula, northern coast of South China Sea, Global Planet. Change, 47, 301–316, <https://doi.org/10.1016/j.gloplacha.2004.10.018>, 2005a.
- Yu, K. F., Zhao, J. X., Wei, G. J., Cheng, X. R., Chen, T. G., Felis, T., Wang, P. X., and Liu, T. S.:  $\delta^{18}\text{O}$ , Sr/Ca and Mg/Ca records of *Porites lutea* corals from Leizhou Peninsula, northern South China Sea, and their applicability as paleoclimatic indicators, Palaeogeogr. Palaeoecol., 218, 57–73, <https://doi.org/10.1016/j.palaeo.2004.12.003>, 2005b.
- Yu, X., Wang, Z., Zhang, H., and Zhao, S.: Impacts of different types and intensities of El Niño events on winter aerosols over China, Sci. Total Environ., 655, 766–780, <https://doi.org/10.1016/j.scitotenv.2018.11.090>, 2019.
- Zhang, H., Cheng, H., Cai, Y., Spötl, C., Kathayat, G., Sinha, A., Edwards, R. L., and Tan, L.: Hydroclimatic variations in southeastern China during the 4.2 ka event reflected by stalagmite records, Clim. Past, 14, 1805–1817, <https://doi.org/10.5194/cp-14-1805-2018>, 2018.